PHYSICAL REVIEW E **80**, 025401(R) (2009)

Finite dissipation and intermittency in magnetohydrodynamics

P. D. Mininni[1,2] and A. Pouquet[1]

[1]*Departamento de Física, Facultad de Ciencias Exactas y Naturales, Universidad de Buenos Aires and CONICET, Ciudad Universitaria, 1428 Buenos Aires, Argentina*

[2]*NCAR, P.O. Box 3000, Boulder, Colorado 80307-3000, USA*

(Received 18 March 2009; published 3 August 2009)

We present an analysis of data stemming from numerical simulations of decaying magnetohydrodynamic (MHD) turbulence up to grid resolution of 1536^3 points and up to Taylor Reynolds number of ~ 1200. The initial conditions are such that the initial velocity and magnetic fields are helical and in equipartition, while their correlation is negligible. Analyzing the data at the peak of dissipation, we show that the dissipation in MHD seems to asymptote to a constant as the Reynolds number increases, thereby strengthening the possibility of fast reconnection events in the solar environment for very large Reynolds numbers. Furthermore, intermittency of MHD flows, as determined by the spectrum of anomalous exponents of structure functions of the velocity and the magnetic field, is stronger than that of fluids, confirming earlier results; however, we also find that there is a measurable difference between the exponents of the velocity and those of the magnetic field, reminiscent of recent solar wind observations. Finally, we discuss the spectral scaling laws that arise in this flow.

DOI: 10.1103/PhysRevE.80.025401 PACS number(s): 95.30.Qd, 96.50.Tf, 47.65.−d, 47.27.Jv

As observations of astrophysical flows become more detailed, the need for a deeper understanding of turbulent flows coupled to magnetic fields grows. An example is the solar wind, a compressible plasma expanding from the sun into the heliosphere which exhibits heating and thermal conduction. In some cases, the magnetohydrodynamic (MHD) approximation may be useful to understand some of these flows, subject to the conditions that the analysis is confined to large scales where a one-fluid approximation may hold and that the velocities are substantially smaller than the speed of light so that displacement currents can be neglected. This latter condition is easily fulfilled, characteristic bulk velocities in the solar wind being typically between 400 and 800 km s^{-1}. The former condition is associated to the fact that the MHD approach cannot describe small scales where kinetic plasma effects become important, such as ambipolar diffusion in weakly ionized plasmas as the interstellar medium or the Hall current for highly ionized media such as the solar wind. In such cases, the nonlinearities of the dynamical equations become more numerous and complex, the parameter space is expanded, and the resulting problem is quite challenging. For that reason, MHD is still a useful approach, albeit a simplified one, to give the lowest-order physical insight into the fate of these flows.

Laboratory experiments have been one venue to understand the physics of such flows, for example, in reconnection [1]. Using liquid metals in the laboratory is a challenge for exploring high magnetic Reynolds numbers R_M because the magnetic Prandtl number $P_M = \nu/\eta$ is small, typically 10^{-6} for sodium (ν and η are the viscosity and magnetic resistivity). A dynamo has been obtained recently within a turbulent flow [2], but the high R_M regime, as is the case for astrophysical flows, remain unattainable in the laboratory. On the other hand, *in situ* observations of the earth environment have grown in importance recently, e.g., with the multispacecraft mission Cluster [3,4]. Observations indicate several features, such as power-law energy spectra [5] and intermittency [6] (see [7] for review). One of the issues is to assess what kind of scaling laws obtains for both the velocity and magnetic fields; moreover, the flow may develop an anisotropic weak turbulence spectrum at small scale as shown in direct numerical simulations (DNSs) [8] and reminiscent of observations in Jupiter's magnetosphere [9].

Indeed, DNS may help but remain challenging in three dimensions. A plethora of results concerning energy spectra in MHD has emerged, with different power laws in different regions of parameter space although the boundaries between these regions are not fully understood. However, whatever the inertial index of the spectrum, one may ask whether, for correlation functions of higher order, similarities between hydrodynamic and MHD turbulence persist. It is already known that it does not in two dimensions [10], MHD being more intermittent than neutral fluids. Results presented here indicate that this is also the case in three dimensions (3D) and that other simplifying assumptions, e.g., that the dissipation rates of kinetic and magnetic energies are equal, may be incorrect.

A further problem concerns the dissipation of energy in the limit of high Reynolds number R_e. Mathematically, this is an open problem in 3D for fluids and MHD, and yet it is central for astrophysics where dissipative structures, reconnection, and acceleration of particles are well observed [3] (note a complete description of these processes goes beyond the MHD approximation). Intermittency (as measured by anomalous exponents of structure functions) and singular behavior are linked since the latter is likely to occur on a set of strong small-scale fluid elements highly localized spatially, be it vortex filaments or current and vorticity sheets. We thus propose in this Rapid Communication an assessment of dissipation, small-scale structures, intermittency, and scaling laws by analyzing a flow computed up to a grid resolution of 1536^3 points.

The incompressible decaying MHD equations read as

$$\partial_t \mathbf{v} + \mathbf{v}\cdot\nabla\mathbf{v} = -\rho_0^{-1}\nabla\mathcal{P} + \mathbf{j}\times\mathbf{b} + \nu\nabla^2\mathbf{v}, \qquad (1)$$

TABLE I. Runs, linear resolution N, viscosity ν, magnetic diffusivity η, Reynolds number (Re), and Taylor Reynolds number R_λ evaluated at peak of dissipation.

Run	N	$\nu=\eta$	Re	R_λ
I	64	8×10^{-3}	390	180
II	128	3×10^{-3}	790	280
III	256	1.25×10^{-3}	1600	430
IV	512	6×10^{-4}	3100	630
V	1536	2×10^{-4}	10500	1180

$$\partial_t \mathbf{b} = \boldsymbol{\nabla} \times (\mathbf{v} \times \mathbf{b}) + \eta \nabla^2 \mathbf{b}, \tag{2}$$

with $\mathbf{v},\mathbf{b}$ as the velocity and magnetic field, $\mathbf{j}=\boldsymbol{\nabla}\times\mathbf{b}$ as the current, $\mathcal{P}$ as the pressure, $\rho_0=1$ as the density, and $\boldsymbol{\nabla}\cdot\mathbf{v}=\boldsymbol{\nabla}\cdot\mathbf{b}=0$. When $\nu=\eta=0$, the energy $E=\langle v^2+b^2\rangle/2$, cross helicity $H_C=\langle\mathbf{v}\cdot\mathbf{b}\rangle/2$, and magnetic helicity $H_b=\langle\mathbf{A}\cdot\mathbf{b}\rangle$ (with $\mathbf{b}=\boldsymbol{\nabla}\times\mathbf{A}$) are conserved. Note that a decaying flow may behave similarly to the forced case at peak of dissipation with quasisteady behavior for some interval of time (see [8]). We solve Eqs. (1) and (2) in a three-dimensional box with periodic boundary conditions and a pseudospectral code dealiased by the 2/3 rule; $k_{\min}=1$ for a box of length $L_0=2\pi$, and N regularly spaced grid points lead to a maximum wave number $k_{\max}=N/3$. At all times, $k_D/k_{\max}<1$, with k_D as the dissipation wave number.

The initial conditions for both the velocity and magnetic fields are constructed from a superposition of Beltrami flows from wave numbers $k=1-3$, to which smaller-scale random fluctuations with a spectrum $k^{-3}\exp[-2(k/k_0)]^2$ for $k>3$ are added (see [8(a)]). The phases of the modes with $k>3$ are chosen from a Gaussian random number generator in such a way that the initial cross correlation of the two fields is negligible: initially, $E_V=E_M=0.5$, $H_C\sim10^{-4}$, and $H_M\sim0.45$. Resolutions of runs described in this Rapid Communication range from $N=64$ to $N=1536$ (see Table I). The largest resolution run is stopped close to the peak of dissipation, $t=3.7$; its initial quasi-ideal phase is described in [8(a)], and the total-energy spectra that develop, together with the ensuing anisotropy of the small scales, is given in [8(b)]. Near the peak of dissipation, the Reynolds number based on the integral scale of the flow velocity is $R_e=UL/\nu\approx9200$, and that it is based on the Taylor scale is $R_\lambda=U\lambda/\nu\approx1700$; U is the rms velocity, the integral scale is defined as $L=2\pi E^{-1}\int k^{-1}E(k)dk$, and the Taylor scale as $\lambda=2\pi[E/\int k^2E(k)dk]^{1/2}$, with $E(k)$ as the total-energy spectra such that $E=\int E(k)dk$.

We focus on the fully developed turbulent regime close to the peak of dissipation. Figure 1 gives the variation in the maximum of the total-energy dissipation rate $\epsilon=\nu\langle\omega^2\rangle+\eta\langle j^2\rangle$ with R_λ ($\boldsymbol{\omega}=\boldsymbol{\nabla}\times\mathbf{v}$ is the vorticity) for the runs of Table I. For large R_λ, ϵ seems to become independent of R_λ. This result is not entirely unexpected. On the one hand, the dissipation of energy is known to tend to a constant in the case of neutral fluids ($\mathbf{b}\equiv0$) [11]; and when restricting the MHD dynamics to 2D (which, to lowest order, is the evolution that is expected in the presence of a strong uniform magnetic field), the energy dissipation was shown similarly to be constant [10]; in three-dimensional MHD, an indication that this may be the case was obtained for the Orszag-Tang vortex [8(a)] although at a lower resolution (512^3 points) and Reynolds number ($R_e\sim5600$). Here, it appears that we have reached the beginning of an asymptotic regime where dissipation is constant and R_λ scales as $R_e^{1/2}$ (see Fig. 1), as expected for a fully developed turbulent flow.

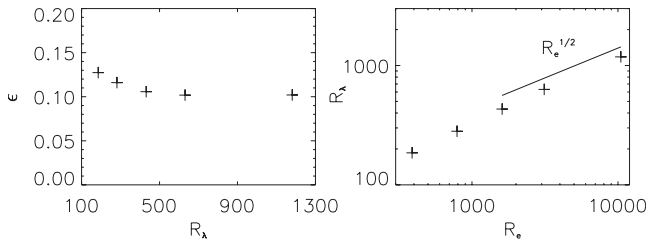

FIG. 1. Left: total-energy dissipation rate ϵ as a function of Taylor Reynolds number R_λ. For large R_λ, ϵ seems to be independent of R_λ. Right: R_λ as a function of R_e calculated at the peak of dissipation for the same runs. The straight line indicates the classical turbulent scaling $R_\lambda\sim R_e^{1/2}$.

For ϵ to remain constant with vanishing viscosity and resistivity, one can think of several scenarios; either we have intense dissipative structures that are more space filling as R_e grows or else the structures remain sparse but become very sharp. Both may be happening, with a myriad of current sheets of intermediate to large intensity and a few very sharp structures. When plotting the histogram of one component of the current intensity (not shown), one observes that, as the Reynolds number increases, the wings of the pair distribution function (PDF) stabilize at intermediate values, but substantially higher extrema are reached. Figure 2 gives a three-dimensional rendering of the current density in a slice of the entire domain and in a subvolume showing folding and rolling of the current sheet. Visualizations of the time evolution of these structures confirm that the rolling takes place as the result of a Kelvin-Helmholtz-like instability. Kelvin-Helmholtz solar wind observations are available at large scales [4], and more resolution would be required to observe rolled structures at small scales where dissipation takes place.

One way to determine the statistics of such features is to examine the behavior of structure functions; at order p for a

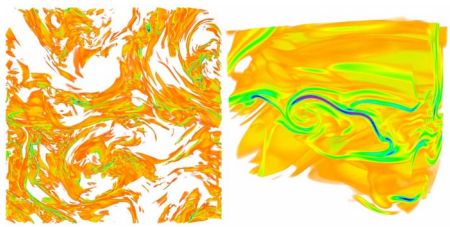

FIG. 2. (Color online) Current density in a slice of the full box (left) and in a subregion (right) showing folding and rolling of the current sheets. Vorticity organizes in the same fashion although current sheets are thinner. High intensity shown in green and magenta (dark gray) is concentrated in thin layers. Three-dimensional visualizations use the VAPOR software [19].

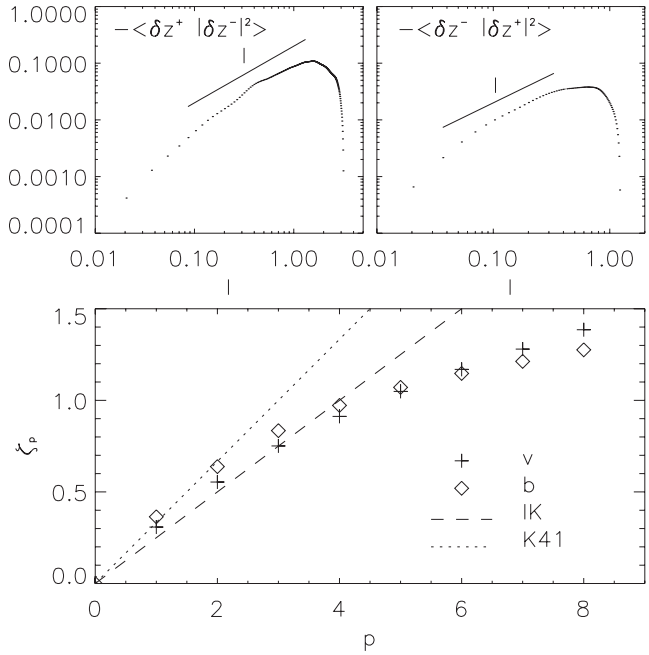

FIG. 3. Top: $-\langle \delta z_{\parallel}^{\mp}(l)|\delta \mathbf{z}^{\mp}(l)|^2\rangle$ as a function of displacement l in the fully developed turbulent regime of the 1536^3 run. A slope of 1 is indicated as a reference. Bottom: scaling exponents ζ_p for the velocity and magnetic fields. The IK and K41 predictions are also shown. Although ζ_2^v is closer to K41 scaling, ζ_3^v is far from the hydrodynamic value of 1. Note the measurable difference between both sets of exponents.

field $\mathbf{u}$, they are defined as $\langle|\delta u_{\parallel}(l)|^p\rangle$, with $\delta u_{\parallel}(l)=u_{\parallel}(\mathbf{x}+\mathbf{l})-u_{\parallel}(\mathbf{x})$ with homogeneity assumed and with $u_{\parallel}$ as the longitudinal component of the vector $\mathbf{u}$ that projects along $\mathbf{l}$. For simplicity, we use here isotropic structure functions although for solar wind turbulence increments parallel and perpendicular to the local magnetic field should be considered (see, e.g., [8]). Assuming self-similarity leads to $\langle|\delta u_{\parallel}(l)|^p\rangle \sim l^{\zeta_p^v}$, with $\zeta_p^v=ap$ for a scale invariant (nonintermittent) field; $a=1/3$ for Kolmogorov scaling (K41 hereafter) and $a=1/4$ for Iroshnikov-Kraichnan (IK hereafter). Departures from such a linear scaling are observed experimentally, observationally, and numerically, but a normal (linear) scaling occurs for third-order functions, expressing the conservation laws of the ideal case: total energy and cross correlation, as well as magnetic helicity [12]. In terms of the Elsässer variables $\mathbf{z}^{\pm}=\mathbf{v}\pm\mathbf{b}$, the first two conservation laws lead to

$$\langle \delta z_{\parallel}^{\mp}(l)|\delta \mathbf{z}^{\pm}(l)|^2\rangle = -\frac{4}{3}\epsilon^{\pm} l, \tag{3}$$

where $\epsilon^{\pm}$ are the dissipation rates of $\mathbf{z}^{\pm}$. From these expressions, the flux of total energy ϵ and of the cross correlation between the fields ϵ_C can be computed. The relations given by Eq. (3) as evaluated directly from the 1536^3 data near the peak of dissipation are shown in Fig. 3. A linear dependence with l is observed in a range of scales for both functions although the scaling is slightly better for the ϵ^- flux; as a result, this is the quantity we will use for the extended self-similarity (ESS) analysis [13]: in fluid turbulence, it is a common practice to plot structure functions in terms of each other, the third-order one being particularly relevant since it is proportional to l and can be used to define the inertial range and to improve the estimation of the scaling exponents. We thus show here the determination of the isotropic exponents for the velocity and magnetic field using ESS. A measurable difference is obtained, reminiscent of observations in the solar wind [14]; it corresponds to a steeper magnetic energy spectrum (close to K41 scaling) and a shallower kinetic energy spectrum (close to IK scaling). Indeed, for the second-order scaling exponent of the velocity field $\zeta_2^v=0.55\pm0.01$ and for the magnetic field $\zeta_2^b=0.64\pm0.01$. These exponents in turn lead to a kinetic energy spectrum $E_v(k)\sim k^{-1.55}$ and a magnetic energy spectrum $E_M(k)\sim k^{-1.64}$. For both fields, $\zeta_3\neq 1$ indicating already at third order a departure from K41 phenomenology. In this simulation the exponents of the Elsässer variables $\mathbf{z}^{\pm}$ are closer to IK scaling than to K41 (with the second-order exponent near 0.6 [8] because of intermittency corrections). Note that the exponents observed in the solar wind are on the average $E(k)\sim k^{-1.6}$, $E_v(k)\sim k^{-1.5}$, and $E_b(k)\sim k^{-1.66}$ [14]. However, comparison must be done with care as the solar wind is highly anisotropic and most fluctuations are perpendicular to the local magnetic field [15].

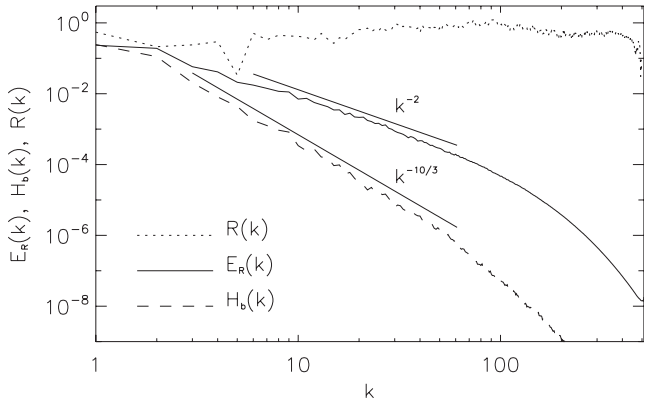

FIG. 4. Residual energy (solid), magnetic helicity (dash), and $R(k)$ (dots, see text) at the peak of dissipation in run V.

The different scaling of the velocity and the magnetic field in MHD can thus be explained in terms of the intermittency properties of each field. Indeed, current sheets are thinner than vortex structures, a property that results in faster dissipation of magnetic energy than of mechanical energy. The development of thin structures in the current in turn leads to a steeper spectrum for the magnetic field than for the velocity field. Other scaling laws arise in the flow, especially at very high R_e, that in some cases have been previously reported in observations or predicted using theoretical arguments. Figure 4 shows the residual energy spectrum $E_R(k)=E_b(k)-E_v(k)$ [16], which for IK scaling should go as k^{-2} and for K41 scaling goes as $k^{-7/3}$; we find $E_R(k)\sim k^{-2}$, consistent with IK scaling. The magnetic helicity H_b seems to follow a $k^{-10/3}$ spectrum. This scaling has also been observed in the inverse cascade range of magnetic helicity [17] and is not well understood. It could result from the Alfvénic balance between $E_b(k)/E_v(k)$ and k^2H_b/H_v [17], where $H_v=\langle \mathbf{v}\cdot\boldsymbol{\omega}\rangle$ is the kinetic helicity and where the factor k^2 follows

from dimensional reasons; Fig. 4 also shows $R(k) = [E_b(k)/E_v(k)][k^2 H_b(k)/H_v(k)]^{-1}$, and although a balance is plausible, $R(k)$ is slowly increasing with k.

The measurement of the energy input ϵ (and ensuing heating) in magnetospheric plasmas is an outstanding problem that the present Cluster mission helps unravel and that future missions, such as the Magnetospheric Multiscale (MMS) to be launched in 2014 is designed for study. From solar wind observations, ϵ can be measured by using the exact scaling laws used here. The fact that the present Rapid Communication shows the constancy of ϵ with Reynolds number indicates that energy can be transferred efficiently to small scales by MHD mechanisms as long as sufficient scale separation is available. In astrophysical plasmas, kinetic plasmas effects will come into play as the cascade meets, e.g., the ion-cyclotron frequency, leaving open the issue of what follows at smaller scales (note that the theoretical framework considered here is a simplified one and cannot be used to understand, e.g., the change in slope of the energy spectrum near the ion-cyclotron frequency observed in the solar wind). Dissipation in MHD is achieved in localized regions with strong magnetic field gradients, in the form of current sheets. These extreme events, more probable at small scales than what is expected from a normal distribution, represent a breakdown of scale invariance and give rise to intermittency. The thin current sheets result in a magnetic field more intermittent than the velocity and in turn make the magnetic energy spectrum steeper than the kinetic energy spectrum. The thin sheets also result in a faster dissipation of magnetic energy than of kinetic energy; this may also shed some light on the observed evolution of the energy spectra with heliospheric distance in the solar wind. Remarkably, the second-order scaling exponents and spectral indices for the kinetic, magnetic, and total energies in the MHD run at the largest Reynolds number are close to the ones reported for the solar wind. However, care must be taken when extracting conclusions about scaling laws in MHD turbulence. The solar wind is highly anisotropic, and the simulations considered here neglect compressibility and kinetic effects. MHD simulations with a strong imposed field have also been reported where the total-energy spectrum follows different power laws depending on properties of the forcing [18], and in the solar wind variations in the total-energy spectrum from $\sim k^{-3/2}$ to $\sim k^{-5/3}$ have been observed [14]. It is not our intention to say that MHD turbulence has unique scaling properties represented by our simulations or that it provides a complete description of space plasmas but rather that the determination of scaling laws in MHD turbulence and the explanation of the results from solar wind observations require the study of often neglected phenomena as intermittency and the measurement of high-order statistics of the velocity and the magnetic fields.

The largest run was performed through a BTS grant at NCAR sponsored by NSF. P.D.M. acknowledges support from UBACYT Grant No. X468/08.

[1] W. Gekelman and R. Stenzel, J. Geophys. Res. **89**, 2715 (1984); M. Yamada *et al.*, Phys. Plasmas **4**, 1936 (1997).
[2] R. Monchaux *et al.*, Phys. Rev. Lett. **98**, 044502 (2007).
[3] C. Cattell *et al.*, J. Geophys. Res. **110**, A01211 (2005); J. R. Wygant *et al.*, *ibid.* **110**, A09206 (2005); A. Retinò *et al.*, Nat. Phys. **3**, 235 (2007).
[4] O. Alexandrova *et al.*, J. Geophys. Res. **109**, A05207 (2004); K. Nykyri *et al.*, Ann. Geophys. **24**, 2619 (2006).
[5] W. H. Matthaeus and M. L. Goldstein, J. Geophys. Res. **87**, 6011 (1982).
[6] L. F. Burlaga, J. Geophys. Res. **96**, 5847 (1991).
[7] C. Tu and E. Marsch, J. Geophys. Res. **95**, 4337 (1990); Y. Zhou, W. H. Matthaeus, and P. Dmitruk, Rev. Mod. Phys. **76**, 1015 (2004).
[8] (a) P. D. Mininni, A. G. Pouquet, and D. C. Montgomery, Phys. Rev. Lett. **97**, 244503 (2006); (b) **99**, 254502 (2007).
[9] J. Saur *et al.*, Astron. Astrophys. **386**, 699 (2002).
[10] H. Politano, A. Pouquet, and P. L. Sulem, Phys. Fluids B **1**, 2330 (1989); D. Biskamp and H. Welter, *ibid.* **1**, 1964 (1989); L. Sorriso-Valvo *et al.*, Europhys. Lett. **51**, 520 (2000).
[11] Y. Kaneda *et al.*, Phys. Fluids **15**, L21 (2003).
[12] H. Politano and A. Pouquet, Geophys. Res. Lett. **25**, 273 (1998); H. Politano, T. Gomez, and A. Pouquet, Phys. Rev. E **68**, 026315 (2003).
[13] R. Benzi *et al.*, Phys. Rev. E **48**, R29 (1993).
[14] J. J. Podesta, D. A. Roberts, and M. L. Goldstein, Astrophys. J. **664**, 543 (2007).
[15] W. Matthaeus, M. Goldstein, and D. Roberts, J. Geophys. Res. **95**, 20673 (1990).
[16] R. Grappin *et al.*, Astron. Astrophys. **105**, 6 (1982); W. C. Müller and R. Grappin, Phys. Rev. Lett. **95**, 114502 (2005).
[17] W. C. Müller (private communication).
[18] P. Dmitruk, D. O. Gómez, and W. H. Matthaeus, Phys. Plasmas **10**, 3584 (2003).
[19] J. Clyne *et al.*, New J. Phys. **9**, 301 (2007).